Process modelling, design and technoeconomic LLE optimisation for comparative evaluation of batch vs. continuous pharmaceutical manufacturing of atropine

PROCESS MODELLING, DESIGN AND TECHNOECONOMIC LIQUID-LIQUID EXTRACTION (LLE) OPTIMISATION FOR COMPARATIVE EVALUATION OF BATCH VS. CONTINUOUS PHARMACEUTICAL MANUFACTURING OF ATROPINE

Samir Diab[a], Nikolaos Mytis[b], Andreas G. Boudouvis[b], Dimitrios I. Gerogiorgis[a*]

[a] Institute for Materials and Processes (IMP), School of Engineering, University of Edinburgh, The Kings Buildings, Edinburgh, EH9 3FB, Scotland, U.K.

[b] School of Chemical Engineering, National Technical University of Athens, Athens 15780, Greece

[*]*Corresponding Author*: D.Gerogiorgis@ed.ac.uk (*+44 131 6517072*)

Keywords: Continuous Pharmaceutical Manufacturing (CPM); Atropine; Process design; Process optimisation; Reactor design; Liquid-Liquid Extraction (LLE)

ABSTRACT

Continuous Pharmaceutical Manufacturing (CPM) can revolutionise industrial efficiency via potential operational and economic benefits over currently dominant batch methods. Process modelling and optimisation are valuable towards rapid design space evaluation and elucidation of optimal process design configurations, without expensive and time-consuming experimental campaigns. This paper pursues total cost minimisation via nonlinear optimisation of different separation design options for atropine, a product of great societal importance. The study considers a demonstrated continuous flow synthesis, presents reaction kinetic parameter estimation towards reactor design, and illustrates a comparative analysis of the subsequent batch vs. continuous Liquid-Liquid Extraction (LLE) for product purification, using published partition coefficient data and UNIFAC-modelled ternary liquid-liquid equilibria. Original optimisation results show that toluene is the best continuous LLE solvent, attaining the lowest total costs at both plant capacities considered and the greatest total cost savings with respect to batch LLE design for varying solvent recovery, at acceptable material efficiencies.

1. Introduction

The pharmaceutical industry produces a wide variety of products whose active pharmaceutical ingredients (APIs) often have complex molecular structures, requiring multistep syntheses (Baumann and Baxendale, 2015) and stringent product purities set by regulatory bodies (Eger and Mahlich, 2014). Such requirements imply materially-intensive manufacturing processes, which can also be very wasteful and have low operational asset efficiencies (Henderson *et al.*, 2011; Anderson, 2012). Consequently, pharmaceutical R&D costs have been historically increasing (DiMasi, Grabowski and Hansen, 2016), characterised by fewer new therapeutic discoveries per R&D expenditure (Plenge, 2016). While total pharmaceutical sales in Europe have been historically increasing, R&D expenditures remain high; in the UK, pharmaceutical R&D has been the highest of all manufacturing sectors for several years, representing nearly 25% of the total national R&D expenditure (Fig. 1). Additionally, competition from generics manufacturers has been historically increasing and is predicted to continue (Fig. 2), presenting a threat to pharmaceutical firm profitability. Manufacturing costs represent a significant portion of expenditures; thus, improved process efficiencies will have significant economic benefits (Rantanen and Khinast, 2015).

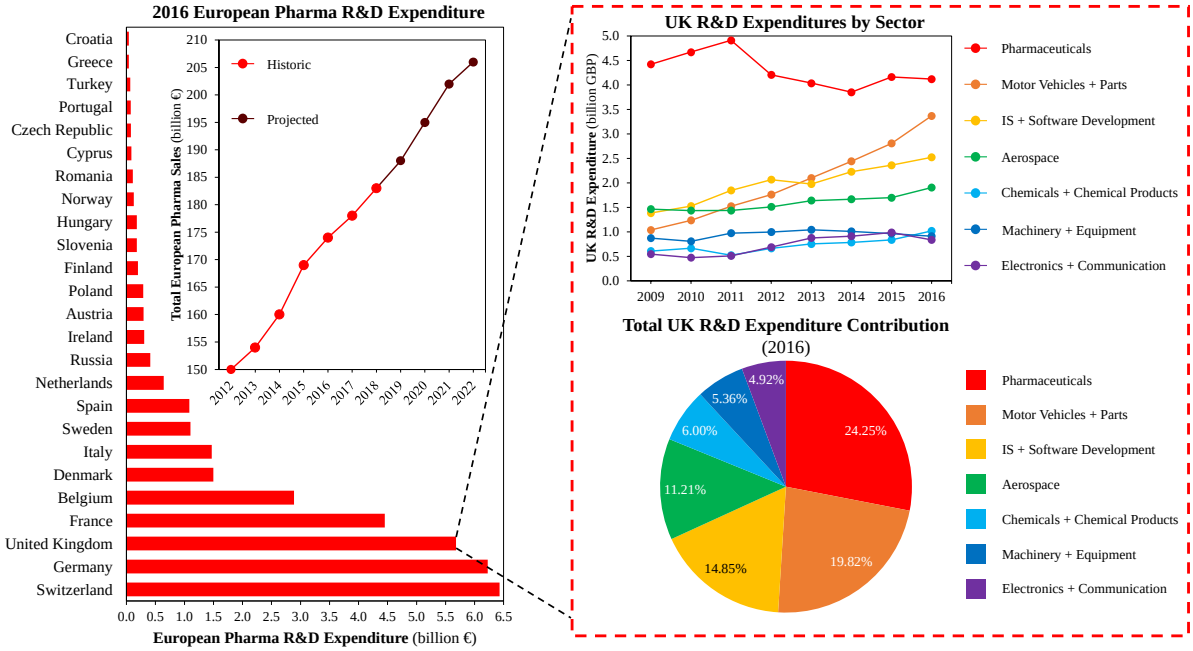

Figure 1: European pharma R&D expenditures and total sales and UK pharmaceutical manufacturing R&D trends by sector (Iervolino, 2016; UK Office for National Statistics, 2016; EFPIA, 2018).

Continuous pharmaceutical manufacturing (CPM) is a new production paradigm for the pharmaceutical industry with the potential to revolutionise production by offering enhanced yields, purities, heat and mass transfer and mixing efficiencies, reduced waste and lower total costs (Jolliffe and Gerogiorgis, 2016; Dallinger and Kappe, 2017). While traditional batch methods have been historically implemented for their advantages of equipment flexibility, product recall ability, utility for rapid synthetic pathway discovery and having established, well-understood technology, batch techniques imply significant waste and low operational asset efficiency, leading to a lack of robustness and flexibility which has lead to drug shortages, presenting a threat to public health (Lee *et al.*, 2015; Yu and Kopcha, 2017). Despite numerous demonstrations of continuous flow synthetic routes towards APIs (Britton *et al.*, 2017; Plutschack *et al.*, 2017), including pilot plant demonstrations (Mascia *et al.*, 2013; Adamo *et al.*, 2016; Cole *et al.*, 2017) and industrial scale applications (GSK, 2015; Kuehn, 2015) and receiving approval from regulatory bodies (Poechlauer *et al.*, 2013), there is wide-scale reluctance to adopt CPM over current batch methods due to significant investments in existing infrastructures (Federsel, 2013). Furthermore, development and integration of robust continuous separation technologies as part of end-to-end campaigns is essential for successful

CPM implementation (Baxendale *et al.*, 2015). Demonstration of feasible and viable CPM processes is essential to maintain sustainable pharmaceutical manufacturing practices.

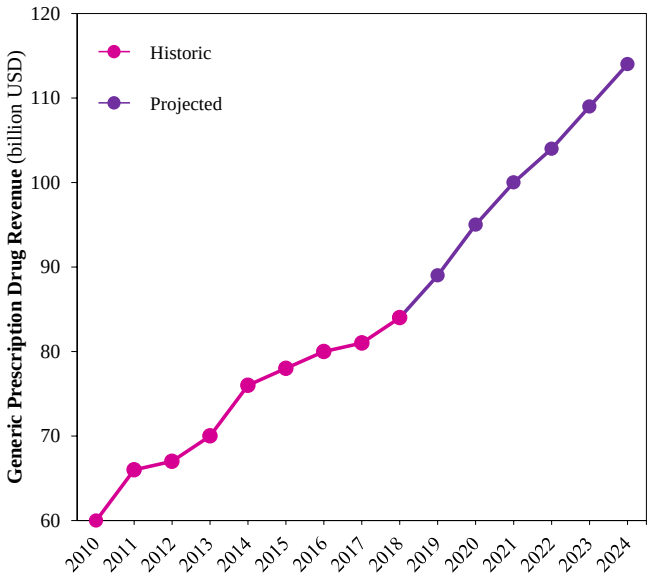

Figure 2: Increasing global generics prescription drug revenues (EvaluatePharma, 2018).

Successful CPM implementation requires the selection of viable candidate APIs whose continuous flow synthesis has been demonstrated in the literature for CPM application. Atropine is a World Health Organisation (WHO) essential medicine, primarily used for the treatment of the effects of nerve agents and poisons, often being the most readily available patient treatment in warzones where chemical warfare is used (Marrs and Rice, 2016). Atropine is also used to induce cycloplegia and mydriasis for ophthalmic treatments, for the treatment of bradycardia and to inhibit salivary and mucus glands during medical procedures (Field *et al.*, 2010). The continuous flow synthesis of atropine was recently demonstrated, featuring two plug flow reactor (PFRs) followed by a purification via liquid-liquid extraction (LLE), partitioning structurally similar impurities between organic and aqueous product phases of a multiphase mixture (Bédard *et al.*, 2016); the study showed an improved material efficiency over previous demonstrations (Dai *et al.*, 2015). Systematic comparative evaluation of process alternatives for operational feasibility and economic viability for atropine CPM has yet to be conducted and can elucidate designs of improved economic viability.

Process modelling, simulation and optimisation is a valid method for rapid systematic comparative evaluation of design alternatives prior to significant financial investments in pilot plant studies (Poku et al., 2004; Angelopoulos *et al.*, 2014; Teoh, Rathi and Sharratt, 2015; Bana *et al.*, 2017). Theoretical methods have been widely implemented in the plantwide design and optimisation of pharmaceutical manufacturing processes to elucidate optimal designs (Rogers and Ierapetritou, 2014; Sahlodin and Barton, 2015; Escotet-Espinoza, Rogers and Ierapetritou, 2016; Patrascu and Barton, 2018). Significant efforts in modelling and simulation in pursuit of continuous pharmaceutical separation process development have been demonstrated in recent years. Implementation of combined experimental and modelling approaches towards integrated LLE design in the literature for pharmaceutical purifications and separations demonstrate the utility of theoretical methods in establishing optimal design and operating parameters (Drageset and Bjørsvik, 2016; Monbaliu *et al.*, 2016; Weeranoppanant *et al.*, 2017). Mathematical optimisation can be used to identify cost optimal process designs for pharmaceutical manufacturing campaigns (Gross and Roosen, 1998; Patrascu and Barton, 2018); plantwide modelling and optimisation with a focus on optimal continuous separation process design towards total cost minimisation have been implemented by our group for numerous APIs (Jolliffe and Gerogiorgis, 2017a,b; Diab and Gerogiorgis, 2018b). Elucidating cost-optimal designs for atropine CPM will further aid process development for this societally-important API.

This work develops a process model for total cost minimisation via nonlinear optimisation of the CPM of atropine based upon the most recently published continuous flow synthesis (Bédard *et al.*,

2016). The design and optimisation of multiphase flow systems to ensure high performance bears exceptional importance for many industries (Grujicic and Chittajallu, 2004); beyond first-principles approaches, statistical methods are useful towards closure (Ma et al., 2015; Tryggvason et al., 2016). Kinetic parameter estimation from published experimental data is implemented for the design of PFRs. The experimentally demonstrated batch LLE is compared to a conceptual continuous LLE for the purification of the PFR effluent, for which LLE model development and plantwide design variation considerations are described. Methods for cost estimation for pharmaceutical processes from the literature are then described. The formulation of the constrained nonlinear optimisation problem for total cost minimisation of the CPM process is then discussed. Optimal operating and design parameters for different process configurations and design assumptions are then provided, with a critical discussion of optimisation results, methods and assumptions made. Future work for the development of the CPM of atropine are discussed, highlighting the utility of process modelling and optimisation studies towards the rapid development of feasible and viable API manufacturing routes.

2. Process Modelling, Simulation and Optimisation

2.1 API Continuous Flow Synthesis

The continuous flow synthesis of atropine is that demonstrated by Bédard *et al.* (2016). The route features three reactions occurring in two PFRs (Fig. 3). The first reactor (PFR-1) features the esterification of tropine **2** (in DMF carrier solvent) and phenylacetyl chloride **3** at 100 °C to form tropine ester HCl **4** (reaction 1), the free form of which (tropine ester **5**) is formed by the addition of NaOH. The second reactor (PFR-2) features an aldol addition of formaldehyde (CH_2O) to **5** (reaction 2a) under basic conditions at 100 °C, giving the desired API product. An undesired elimination of API to apoatropine **6** (reaction 2b, PFR-2) is also reported (Bédard *et al.*, 2016).

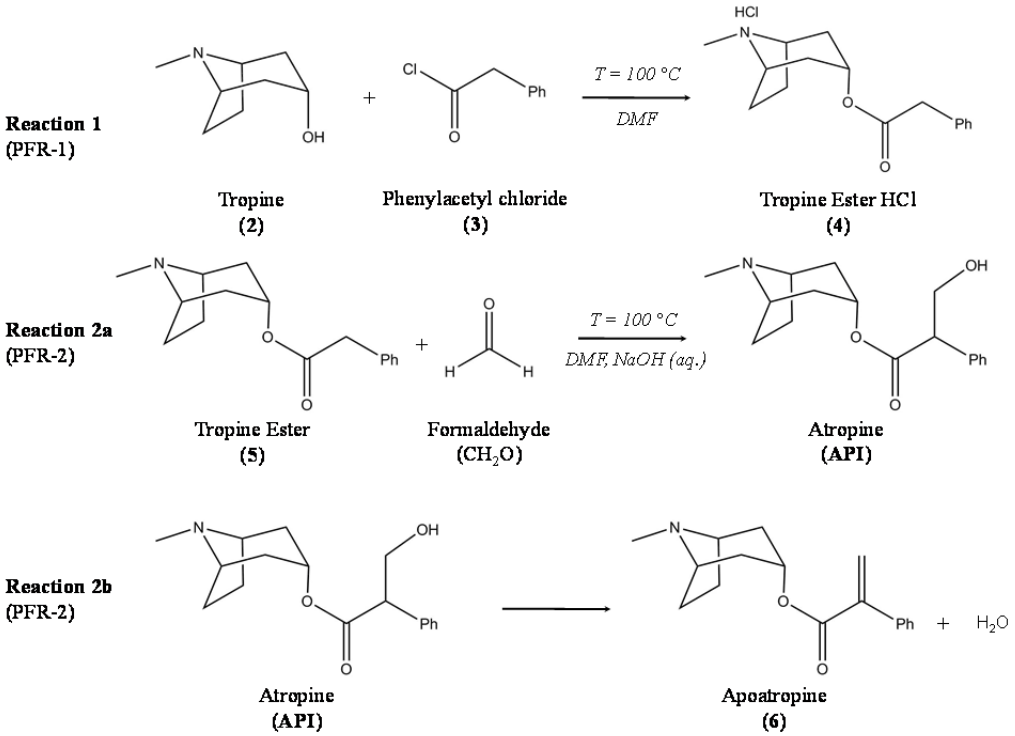

Figure 3: Reaction scheme of the demonstrated API continuous flow synthesis (Bédard *et al.*, 2016).

2.2 Process Flowsheet

The process flowsheet for atropine CPM considered in this work is shown in Fig. 4; physical properties of all materials used in continuous flow syntheses and subsequent separation process designs are listed in Table 1. A mixture of 1.0 equiv. tropine **2** (2 M in DMF) and 1.0 equiv. neat phenylacetyl chloride **3** undergo esterification at 100 °C in PFR-1. A NaOH solution (1.2 equiv., 3 M aq.) is added to the effluent of PFR-1. Formaldehyde is added to the process mixture (6.0 equiv., 37%

w/v aq.) before entering PFR-2 where the aldol reaction occurs at 100 °C. The batch (BX-) or continuous (CPM-) LLE process is operated at T_{LLE} = 25 °C and is further described in section 2.3.3.

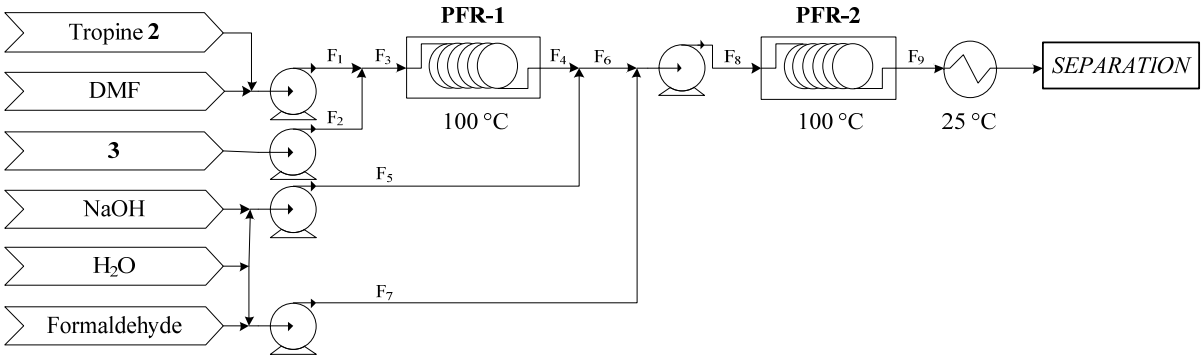

Figure 4: Process flowsheet for CPM of atropine (Bédard *et al.*, 2016).

2.3 Process Modelling and Nonlinear Optimisation

2.3.1 Reaction Performances and Kinetic Parameter Estimation

Kinetic parameter estimation from available experimental reaction performance data should be implemented where possible to gain an understanding of the kinetic behaviour of different reactions and for accurate PFR sizing. For the esterification reaction, the published continuous flow synthesis reports 99% conversion to **4** at 100 °C in a residence time of 3.5 min (Bédard *et al.*, 2016). As time-dependent kinetic data is not available for this reaction, this work assumes the same reported performance; given the availability of a wider dataset for this reaction, kinetic parameter estimation can be performed, which will deepen insight into its kinetic behaviour.

Table 1: Component physical properties.

Type	Component	CAS #	Formula	MW (g mol^{-1})	m.p. (°C)	b.p. (°C)	ρ (g cm^{-3})	μ (mPa s)
Reagent	Tropine **2**	120-29-6	$C_8H_{15}NO$	141.21	64.0	233.0	1.02	–
	DMF	68-12-2	C_3H_7NO	73.09	-60.5	153.0	0.95	0.92
	Phenylacetyl chloride **3**	103-80-0	C_8H_7ClO	154.59	–	94.5	1.17	–
	Sodium hydroxide	1310-73-2	NaOH	40.00	318.0	1,388.0	2.13	–
	Water	7732-18-5	H_2O	18.02	100.0	0.0	1.00	1.00
	Formaldehyde	50-00-0	CH_2O	30.03	-92.0	-19.0	0.82	–
	API	51-55-8	$C_{17}H_{23}NO_3$	289.37	118.5	–	1.21	–
	Apoatropine **6**	207-906-7	$C_{17}H_{21}NO_2$	271.36	62.0	–	–	–
	Hydrogen chloride	7647-01-0	HCl	36.46	-114.2	-85.1	1.49	–
LLE Component	Ammonium chloride	12125-02-9	NH_4Cl	53.94	338.0	520	1.52	–
	Dichloromethane, DCM	75-09-2	CH_2Cl_2	84.93	-96.7	39.6	1.33	0.43
	Diethyl ether, Et_2O	60-29-7	$C_4H_{10}O$	74.12	-116.3	34.6	0.71	0.22
	n-butyl acetate, *n*-BuOAc	123-86-4	$C_6H_{12}O$	116.16	-78.0	126.1	0.88	0.69
	Toluene	108-88-3	C_7H_8	92.14	-95.0	111.0	0.87	0.59

For the aldol addition, conversions of **5** of 67% and 78% are attained after 8 min and 24 min, respectively, at 100 °C, using 6.0. equiv. formaldehyde with 1.2 equiv. NaOH (3 M aq.) added to the effluent of PFR-1 prior to entering PFR-2 (Bédard *et al.*, 2016). This data is used to compare candidate rate law expressions for PFR-2; by plotting different functions of reagent (**5** and formaldehyde) concentrations vs. time, coefficients of determination (R^2) are estimated to determine the goodness of fit of candidate rate law expressions. Zero-order, first-order in limiting reagent **5** and overall second-order (first-order in **5**, first-order in formaldehyde) rate law expressions are considered. The integral forms of the zero-, first- and second-order rate laws are written as eqs. 1–3, respectively; these give linear functions of reagent concentration vs. time from which reaction rate constants can be estimated. Here, C_5 and C_{CH_2O} are the concentrations of **5** and formaldehyde (excess

reagent), respectively, at time τ_{PFR}; $C_{i,0}$ is the initial concentration of i and k_j is the j^{th}-order rate constant.

$$C_{\mathbf{5}} = C_{\mathbf{5},0} - k_0\tau_{PFR} \quad (1)$$

$$\ln\left(\frac{C_{\mathbf{5}}}{C_{\mathbf{5},0}}\right) = -k_1\tau_{PFR} \quad (2)$$

$$\ln\left(\frac{C_{\mathbf{5},0}C_{CH_2O}}{C_{\mathbf{5}}C_{CH_2O,0}}\right) = k_2\left(C_{CH_2O,0} - C_{\mathbf{5},0}\right)\tau_{PFR} \quad (3)$$

Functions of reagent concentrations vs. time representing candidate rate law expressions considered here are plotted in Fig. 5. An overall second-order (first in **5**, first in formaldehyde) rate law is the most plausible case (R^2 = 0.890), followed by a first-order rate law (R^2 = 0.670), followed by a zero-order rate law (R^2 = 0.512) of the candidate rate law expressions considered here. The second-order rate law constant for the aldol addition reaction is estimated as k_2 = 1.68 L mol^{-1} h^{-1}. Greater availability of kinetic data for this reaction set (Fig. 3) will allow further validation of kinetic parameter estimation results, allow investigation of more complex candidate rate law expressions and allow explicit consideration of the elimination of API to **6**. The dataset should be as large as possible (enough to establish a reliable relationship whilst considering the effects of noise). However, the required experimental effort (time and labour) to generate sufficiently large datasets for multiple reactions remains crucial in kinetic data acquisition, justifying consideration and development of simulation and model optimisation methods to aid such efforts (Gillespie, 2008; Grom *et al.*, 2016); a recent focus on statistical methods is noted (Goh et al., 2017). Conversely, modelling via limited datasets can aid R&D decision-making with cost-effective experimentation (especially when disproving flowsheets, thereby entirely circumventing costly and laborious experimental campaigns). From the published data, approximately 39.2% of API formed is eliminated to **6**; this is considered in mass balance and PFR sizing calculations to obtain process performance and equipment sizing results.

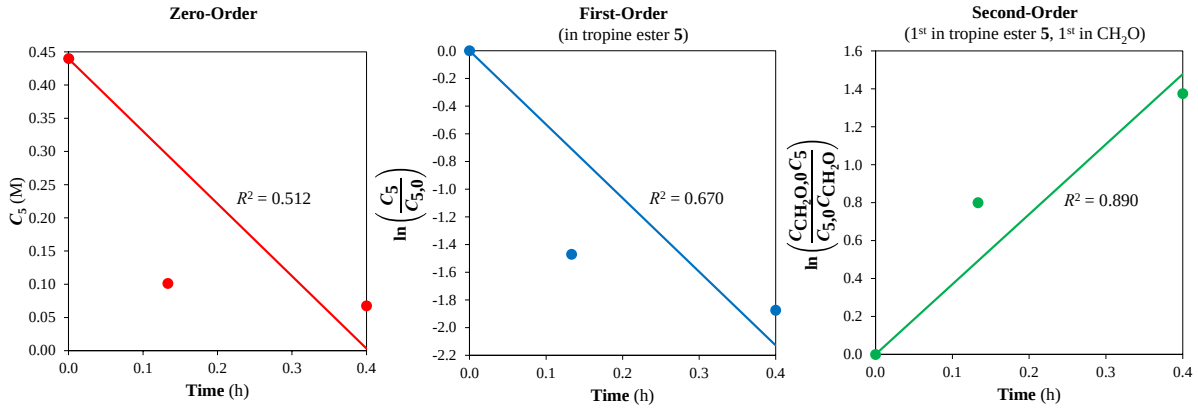

Figure 5: Comparison of candidate rate law expressions for the aldol addition vs. experimental data.

2.3.2 Plug Flow Reactor (PFR) Design

The volume of PFR-1, V_{PFR1}, is estimated from the required residence time required to reach 99% conversion of **2**, τ_{PFR1} = 3.5 min (Bédard *et al.*, 2016) and the reactor volumetric throughput, Q_{PFR1}.

$$V_{PFRi} = \tau_{PFRi}Q_{PFRi} \quad (4)$$

Having established the second-order (first in **5**, first in formaldehyde) rate constant, k_2, for the aldol addition, the PFR-2 residence time required to attain a reported maximum conversion of **5**, X_5 = 78% (Bédard *et al.*, 2016) is calculated (eq. 5).

$$\tau_{PFR2} = \frac{1}{k_2 C_{5,0}} \int_0^{X_5} \frac{dX_5}{(1 - X_5)(\Theta_{CH_2O} + \nu_{CH_2O} X_5)} \quad (5)$$

Here, X_5 is the conversion of **5**, Θ_{CH_2O} is the molar ratio of excess (formaldehyde) to limiting reagent (**5**) and ν_{CH_2O} is the stoichiometric coefficient of CH_2O (= –1). The volume of PFR-2, V_{PFR2}, is then estimated from the residence time (τ_{PFR2}) and the reactor volumetric throughput, Q_{PFR2}, as per eq. 4.

2.3.3 Separation Process Design

Batch (BX-) and continuous (CPM)-LLE configurations are compared for their operational and economical performances following the API continuous flow synthesis considered in this work (Bédard *et al.*, 2016). Description of the experimentally demonstrated BX-LLE is provided in section 2.3.3.1; conceptual CPM-LLE processes modelled in this work are described in section 2.3.3.2.

For both BX- and CPM-LLE considerations, process performances at multiple plant API capacities, Q_{API} = {10^3, 10^4} kg API yr^{-1}, are compared; this is useful in theoretical modelling studies in the early stages of process development to elucidate process performance on different operating scales (Jolliffe and Gerogiorgis, 2016). We also consider different assumptions of attainable solvent recovery, *SR* = {30, 50, 70}%; solvent constitutes a major contribution of material in the CPM process considered here, and thus differences in attainable solvent recovery are an important design consideration.

2.3.3.1 Batch Liquid-Liquid Extraction (BX-LLE)

The flowsheet for the BX-LLE process described in the literature (Bédard *et al.*, 2016) is shown in Fig. 6; the process is implemented following the continuous flow synthesis process described previously (flowsheet provided in Fig. 4). The PFR-2 effluent is altered to pH = 6.5 with a NH_4Cl buffer solution (aq.) with diethyl ether (Et_2O) as LLE solvent; under these conditions, impurities **5** and **6** partition in the organic phase (waste) while API and **2** remain in the aqueous phase. The aqueous phase of this process then undergoes an additional extraction using dichloromethane (DCM) at pH = 10, where API selectively partitions into an organic (product) phase and **2** remains in the aqueous (waste) phase. The BX-LLE process attains a reported API recovery of 99% (Bédard *et al.*, 2016). The considered BX-LLE process includes all essential reported purification steps as reported in the literature, but not considering steps associated with LLE phase solute content monitoring and characterisation; this is to ensure as uniform a comparison between BX-LLE and CPM-LLE processes as possible.

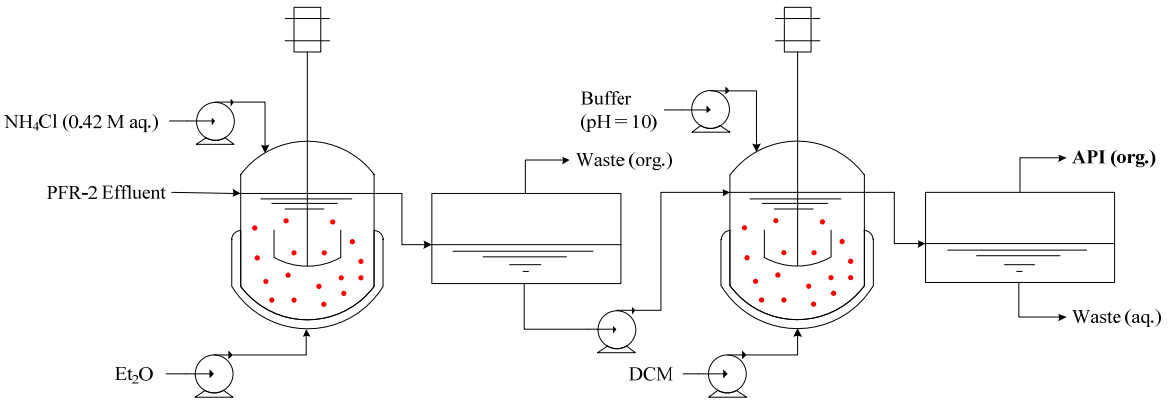

Figure 6: Batch liquid-liquid extraction (BX-LLE) flowsheet based on the experimental demonstration (Bédard *et al.*, 2016).

2.3.3.1 Continuous Liquid-Liquid Extraction (CPM-LLE) Design Configurations

The design of a continuous purification and separation processes is essential to realise the benefits of fully end-to-end CPM. The experimental API continuous flow synthesis demonstration described a possible continuous separation in which the PFR-2 effluent is altered to pH = 6.5 and toluene is added

as a LLE solvent to induce phase splitting (Bédard *et al.*, 2016). The resulting mixture is passed through a packed bed (containing either sand or stainless steel beads) and a subsequent Zaiput membrane separator to yield an aqueous (product) phase rich in API with residual **2** from reaction 1 and an organic (waste) phase rich in impurities **5** and **6**. Modelling of flow characteristics and scaling of the packed bed is not possible from published data and performance of the implemented membrane separator is unknown (Bédard *et al.*, 2016). Furthermore, the feasibility of implementing of packed beds and the described membrane separator on larger production scales is not certain. Therefore, we have explored an alternative conceptual continuous LLE (CPM-LLE) for comparison with the described BX-LLE.

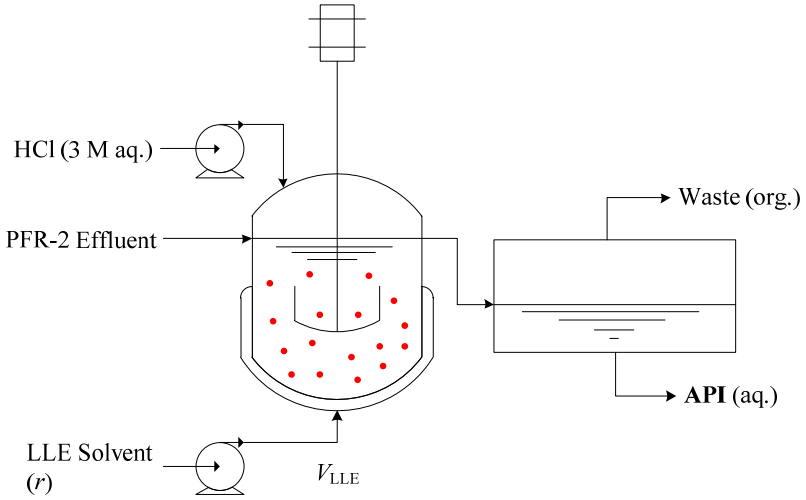

Figure 7: Conceptual continuous liquid-liquid extraction (CPM-LLE).

We consider a conceptual CPM-LLE for the purification of the aqueous PFR-2 effluent under neutral conditions (pH = 7); the flowsheet for the continuous LLE modelled in this work is shown in Fig. 7. The effluent of PFR-2 is neutralised using 3 M HCl (aq.) solution. A candidate LLE solvent is added to the mixture to induce phase splitting. The LLE phases are then separated, producing an aqueous phase rich in API and residual **2** and an organic phase containing impurities (waste).

Modelling of candidate CPM-LLE designs requires liquid-liquid equilibria data for the solvent system DMF + H_2O + LLE solvent and an estimation of partitioning behaviour of various solutes (API + impurities) between LLE phases. The LLE solvents considered for implementation in this work are diethyl ether (Et_2O), *n*-butyl acetate (*n*-BuOAc) and toluene; the shortlisting of these solvents for their liquid-liquid equilibria characteristics and availability of solute partitioning data in these solvent systems are discussed further in sections 2.3.3.3 and 2.3.3.4, respectively.

2.3.3.3 Ternary Phase Compositions and Solute Partitioning

Candidate CPM-LLE solvents must have a high propensity to form multiphase mixtures; diethyl ether (Et_2O), *n*-butyl acetate (*n*-BuOAc) and toluene exhibit rapid phase splitting in a wide range of operating regions upon addition to the aqueous PFR-2 effluent (DMF + H_2O) mixture. Estimation of LLE phase compositions are required for calculation of LLE phase properties (densities, viscosities, surface tensions) for LLE efficiency estimation (described in section 2.3.3.4). The popular UNIFAC model is used for the calculation of liquid-liquid equilibria phase compositions of different LLE solvent systems (Fredenslund, Jones and Prausnitz, 1975). Ternary phase diagrams for different LLE solvent systems of are illustrated in Fig. 8. Varying the LLE solvent-to-feed ratio (*r*, mass basis) affects resulting phase compositions, quantities and physical properties that subsequently affect LLE efficiency.

To avoid explicit phase composition calculation via the UNIFAC model in the problem formulation (which would considerably increase computational effort), extensive preparatory UNIFAC simulations have been performed. Eq. 6 is an empirical polynomial to express the mole fraction of each component calculated via the UNIFAC model for both organic and aqueous phases of the ternary

solvent system as a function of the solvent-to-feed ratio (r), for which $R^2 > 0.96$. Coefficients for eq. 6 (listed in Table 2) have been estimated via nonlinear regression for estimation of phase compositions required for continuous LLE modelling.

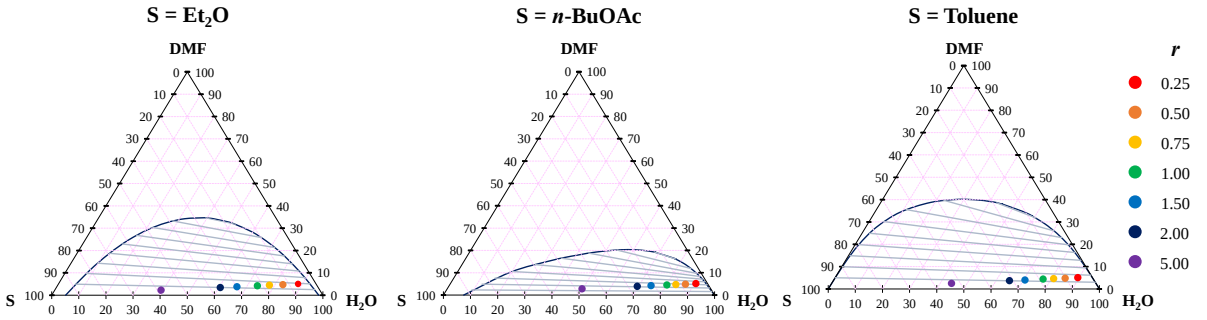

Figure 8: UNIFAC-modelled ternary phase diagrams of the system DMF + H_2O + LLE Solvent (S) with example operating points (LLE solvent-to-feed ratios, r).

$$x_{iS}^{j} = \alpha_{iS}^{j} r^2 + \beta_{iS}^{j} r + \gamma_{iS}^{j} \quad (6)$$

Here, x_{iS}^{j} is the mole fraction of component i in phase j for solvent system DMF + H_2O + LLE solvent (S). Table 2 provides coefficient values for eq. 6 for each solvent system, solvent component and phase.

Table 2: Coefficients for eq. 6 estimating ternary phase compositions of the system DMF + H_2O + LLE solvent (S) based upon extensive UNIFAC modelling.

LLE Solvent (S)		**Et_2O**			***n*-BuOAc**			**Toluene**		
Phase	**Component**	α	β	γ	α	β	γ	α	β	γ
Org.	DMF	$5.50\cdot10^{-3}$	$-4.66\cdot10^{-2}$	$1.11\cdot10^{-1}$	$-9.00\cdot10^{-4}$	$-5.10\cdot10^{-4}$	$7.78\cdot10^{-2}$	$2.90\cdot10^{-3}$	$-2.37\cdot10^{-2}$	$8.57\cdot10^{-2}$
	H_2O	$1.80\cdot10^{-3}$	$-1.70\cdot10^{-2}$	$9.05\cdot10^{-2}$	$4.40\cdot10^{-3}$	$-3.44\cdot10^{-2}$	$1.76\cdot10^{-1}$	$3.00\cdot10^{-5}$	$-2.00\cdot10^{-4}$	$6.00\cdot10^{-4}$
	S	$-7.20\cdot10^{-3}$	$6.36\cdot10^{-2}$	$7.98\cdot10^{-1}$	$-3.60\cdot10^{-3}$	$3.96\cdot10^{-2}$	$7.46\cdot10^{-1}$	$-2.90\cdot10^{-3}$	$2.39\cdot10^{-2}$	$9.14\cdot10^{-2}$
Aq.	DMF	$3.50\cdot10^{-3}$	$-3.20\cdot10^{-3}$	$-3.00\cdot10^{-4}$	$1.40\cdot10^{-3}$	$-1.35\cdot10^{-2}$	$5.14\cdot10^{-2}$	$9.00\cdot10^{-4}$	$-1.01\cdot10^{-2}$	$4.75\cdot10^{-2}$
	H_2O	$-2.79\cdot10^{-2}$	$2.54\cdot10^{-2}$	$2.50\cdot10^{-3}$	$-4.00\cdot10^{-4}$	$9.10\cdot10^{-3}$	$9.43\cdot10^{-3}$	$-1.10\cdot10^{-3}$	$1.11\cdot10^{-2}$	$9.47\cdot10^{-1}$
	S	$6.18\cdot10^{-2}$	$9.21\cdot10^{-1}$	$1.71\cdot10^{-2}$	$-1.10\cdot10^{-3}$	$4.40\cdot10^{-3}$	$5.50\cdot10^{-3}$	$2.00\cdot10^{-4}$	$-1.00\cdot10^{-3}$	$5.20\cdot10^{-3}$

2.3.3.3 Solute Partitioning in Multiphase LLE Mixtures

Estimation of API and impurities partitioning between organic and aqueous phases is required for the modelling of CPM-LLE of atropine. Partition coefficients of API, **2**, **5** and **6** in different combinations of LLE solvent + H_2O systems at pH = 7 and T_{LLE} = 25 °C based upon extensive SPARC simulations are available in the literature (Bédard *et al.*, 2016). For all CPM-LLE solvent systems, operation at pH = 7 is chosen, for which published partition coefficients for API and **2**, **5** and **6** are provided in Table 3. It is assumed that polar components NaOH and NaCl (byproduct from neutralisation of **4** by NaOH) remain in the aqueous phase, whereas **3** and formaldehyde are assumed to partition completely into the organic phase. Provision of partition coefficient data for those species not listed in Table 3 will allow more accurate estimation of solute component content of LLE phases required for process development of subsequent downstream unit operations.

Table 3: Partition coefficients of API and impurities **2**, **5** and **6** in different solvent systems (S) at pH = 7 based upon published SPARC-derived values (Bédard *et al.*, 2016).

Component	**S = Et_2O**	**S = *n*-BuOAc**	**S = Toluene**
API	0.326	0.359	0.273
Tropine **2**	0.028	0.027	0.021
Tropine Ester **5**	2.054	2.312	2.598
Apoatropine **6**	2.054	3.043	3.486

Component partitioning of API and impurities **2**, **5** and **6** are based upon partition coefficient data assuming pure organic (LLE solvent) and aqueous (water) phases (Bédard *et al.*, 2016). Real LLE phases are not pure components, but multicomponent solvent mixtures, including DMF carrier solvent, and various solutes (API, impurities, other reagents). The presence of DMF and other components are not considered to affect the partition coefficient data used to estimate solute partitioning; consideration of these effects require partition coefficient data in multicomponent mixtures, which is not available. Investigation into the effect of additional component presence on solute partitioning will further elucidate the performance of different LLE designs.

2.3.3.4 Continuous (CPM)-LLE Efficiency and Mass Transfer Correlations

Estimation of LLE efficiencies from appropriate mass transfer correlations is required for consideration of the effect of inefficiencies associated with steady-state (continuous) operation on component partitioning at equilibrium. The LLE efficiency, E_{LLE}, is calculated by eq. 7.

$$E_{\mathrm{LLE}} = \frac{1}{\frac{Q_{\mathrm{LLE}}}{K_{\mathrm{i}} a_{\mathrm{i}} V_{\mathrm{LLE}}} + 1} \tag{7}$$

Here, K_{i} is the overall mass transfer coefficient, Q_{LLE} is the LLE volumetric throughput, a is the interfacial area between phases, and V_{LLE} is the LLE tank volume. K_{i} is calculated from continuous and dispersed phase mass transfer coefficients, k_{c} and k_{d}, respectively, which are calculated by phase Sherwood numbers, Sh_{i} (Skelland and Moeti, 1990).

$$K = \frac{1}{\frac{1}{k_{\mathrm{c}}} + \frac{1}{k_{\mathrm{d}}}} \tag{8}$$

$$Sh_{\mathrm{d}} = \frac{k_{\mathrm{d}} d_{32}}{D_{\mathrm{API,d}}} = 6.6 \tag{9}$$

$$Sh_{\mathrm{c}} = \frac{k_{\mathrm{c}} d_{32}}{D_{\mathrm{API,c}}} = 1.27\times10^{-5} Sc_{\mathrm{c}}^{1/3} Fr_{\mathrm{c}}^{5/12} Eo^{5/4} \phi^{-1/2} Re_{\mathrm{i}}^{2/3} \left(\frac{d_{\mathrm{i}}}{d_{32}}\right)^{2} \left(\frac{d_{32}}{d_{\mathrm{t}}}\right)^{1/2} \tag{10}$$

Here, d_{32} is the Sauter mean droplet diameter, $D_{\mathrm{API,i}}$ is the API molecular diffusivity in phase i (eq. 11), Sc_{c} is the continuous phase Schmidt number (eq. 12), Fr_{c} is the continuous phase Froude number (eq. 13), Eo is the Eotvos number (eq. 14), ϕ is the continuous phase volume fraction, Re_{i} is the LLE tank impeller Reynolds' number (eq. 15) and d_{i} and d_{t} are the impeller and tank inner diameters, respectively, assuming a tank aspect ratio of 1 and a tank-to-impeller diameter ratio of 2.

$$D_{\mathrm{API,i}} = \frac{k_{\mathrm{b}} T_{\mathrm{LLE}}}{6\pi \mu_{\mathrm{i}} r_{\mathrm{API}}} \tag{11}$$

$$Sc_{\mathrm{c}} = \frac{\mu_{\mathrm{c}}}{\rho_{\mathrm{c}} D_{\mathrm{API,c}}} \tag{12}$$

$$Fr_{\mathrm{c}} = \frac{d_{\mathrm{i}} N_{\mathrm{i}}^2}{g} \tag{13}$$

$$Eo = \frac{\rho_{\mathrm{d}} d_{32}^2 g}{\sigma} \tag{14}$$

$$Re_{\mathrm{i}} = \frac{d_{\mathrm{i}}^2 N_{\mathrm{i}} \rho_{\mathrm{m}}}{\mu_{\mathrm{m}}} \tag{15}$$

Here, k_{b} is the Boltzmann constant, T_{LLE} is the LLE operating temperature (25 °C), μ_{i} is the phase viscosity, r_{API} is the API molecular radius, ρ_{i} is the density of phase i, N_{i} is the LLE tank impeller

speed (= 6 r.p.s. in this work), g is acceleration due to gravity, σ is the interphase surface tension, and ρ_m and μ_m are the mixture density and viscosity, respectively. The Sauter mean droplet diameter, d_{32} (eq. 16) depends on the Weber number, We (eq. 17).

$$d_{32} = \begin{cases} 0.052 d_i We^{-0.6} e^{4\phi} & , We < 10^3 \\ 0.390 d_i We^{-0.6} & , We > 10^3 \end{cases} \quad (16)$$

$$We = \frac{d_i^3 N_i^2 \rho_c}{\sigma} \quad (17)$$

$$a = \frac{6\phi}{d_{32}} \quad (18)$$

The Skelland-Moeti correlation implemented for LLE modelling (eqs. 9-17) are established from a large dataset of mass transfer coefficients in continuous agitated liquid-liquid systems with intermediate to high surface tensions (σ) and low dispersed phase volume fraction (ϕ). All solvent systems here have intermediate surface tensions. The volume fractions of dispersed phases of different solvent systems as a function of the LLE solvent-to-feed ratio (r) is shown in Table 4; all values are low to intermediate.

Table 4: Dispersed phased volume fractions (ϕ) as a function of LLE solvent-to-feed ratio (r) for different solvent choices.

S	**Et_2O**		**BuOAc**		**PhMe**	
r	**Dispersed Phase** (Org. / Aq.)	ϕ (%)	**Dispersed Phase** (Org. / Aq.)	ϕ (%)	**Dispersed Phase** (Org. / Aq.)	ϕ (%)
0.25	Org.	26.06	Org.	26.30	Org.	24.57
1	Aq.	37.74	Aq.	38.29	Aq.	42.76
2	Aq.	22.16	Aq.	21.95	Aq.	27.04
3	Aq.	15.46	Aq.	14.74	Aq.	19.70
4	Aq.	11.78	Aq.	10.57	Aq.	15.42
5	Aq.	9.40	Aq.	7.59	Aq.	12.60

2.3.4 Environmental Impact Analysis

Quantities of waste produced by different designs are compared via the popular green chemistry metric, the environmental (E)-factor, defined as the mass ratio of waste to desired product, i.e., recovered API (Sheldon, 2012). Here, m_{waste} is the total mass of waste, m_{API} and m_{uAPI} are the mass of recovered and unrecovered API, respectively, m_{uS} is the mass of unrecovered solvent and m_{ur} is the mass of unreacted reagents.

$$E = \frac{m_{waste}}{m_{API}} = \frac{m_{uAPI} + m_{uS} + m_{ur}}{m_{API}} \quad (19)$$

2.3.5 Costing Methodology

We implement an established methodology for costing pharmaceutical manufacturing processes (Jolliffe and Gerogiorgis, 2016). All plant designs are assumed to be constructed and operated at an existing pharmaceutical manufacturing site with essential auxiliary structures already in place. Annual operation of 8,000 hours is considered.

Prices for equipment of similar capacities to those considered here have been sourced where possible; where such data is unavailable, the following cost-capacity correlation is used (Couper, 2003).

$$P_B = f P_A \left(\frac{S_B}{S_A}\right)^n \quad (20)$$

P_j is the equipment purchase cost at capacity S_j. Parameters n and f are equipment-dependent and can be found in the literature (Woods, 2007). Where the reference purchase cost (P_A) is taken from the

past, chemical engineering plant cost indices (CEPCIs) are used to calculate the corresponding present purchase cost in the present day. All equipment capacities are scaled to account for plantwide inefficiencies to meet the specified plant capacity. Table 5 gives details for the purchase costs and scaling parameters in eq. 20 for each equipment item.

Table 5: Equipment parameters for calculating scaled equipment purchase costs in the present day (eq. 20).

Item	Ref. Year	Ref. Cost, P_A (GBP)	Capacity Basis	Ref. Capacity, S_A	n	f (%)	Ref.
PFR	2014	103,208	V_{PFRi} (mL)	80.00	1.00	1.06	(Corning, 2015)
Pump	2015	958	–	–	–	–	(ProMinent, 2015)
Cooler	2015	3,454	–	–	–	–	(Cole-Parmer, 2015)
Mixer	2007	22,230	Power (kW)	5	0.30	10.33	(Woods, 2007)
LLE	2007	19,500	V_{LLE} (L)	10	0.22	10.33	(Woods, 2007)

The sum of all inflation-adjusted equipment costs (P_B) gives the Free-on-Board (*FOB*) cost. The Chilton method is used to calculate the battery limits installed cost (*BLIC*)(Couper, 2003). The installed equipment cost (*IEC*), process piping and instrumentation (*PPI*) and total physical plant cost (*TPPC*) are calculated from eqs. 21-23. A construction factor of 30% is added to the *TPPC* to calculate the *BLIC* (eq. 24) (Jolliffe and Gerogiorgis, 2016).

$$IEC = 1.43FOB \tag{21}$$
$$PPI = 0.42IEC \tag{22}$$
$$TPPC = IEC + PPI \tag{23}$$
$$BLIC = 1.3TPPC \tag{24}$$

Working capital (*WC*) costs are taken as 35% and 3.5% of annual material costs scaled to meet the desired plant capacity (MAT_{annual}) for batch and continuous processes, respectively (Jolliffe and Gerogiorgis, 2016). Contingency costs (*CC*) are calculated as 20% of the *BLIC*. The sum of *BLIC*, *WC* and *CC* gives the total capital expenditure (*CapEx*).

$$WC = \begin{cases} 0.350MAT_{annual}\text{ , batch} \\ 0.035MAT_{annual}\text{ , CPM} \end{cases} \tag{25}$$
$$CC = 0.2BLIC \tag{26}$$
$$CapEx = BLIC + WC + CC \tag{27}$$

Required material prices are sourced from various vendors and are summarised in Table 6. The annual utilities cost ($UTIL_{annual}$) is calculated as 0.96 GBP kg^{-1} of the process material throughput ($m_{process}$); the annual waste cost ($Waste_{annual}$) is 0.35 GBP L^{-1} of waste produced (Jolliffe and Gerogiorgis, 2016). Annual operating expenditure ($OpEx_{annual}$) is calculated as the sum of annual material (MAT_{annual}), utilities ($UTIL_{annual}$) and waste disposal ($Waste_{annual}$).

$$UTIL_{annual} = 0.96m_{process} \tag{28}$$
$$Waste_{annual} = 0.35Q_{waste} \tag{29}$$
$$OpEx_{annual} = MAT_{annual} + UTIL_{annual} + Waste_{annual} \tag{30}$$

Labour costs are not included in the costing methodology as considered designs are not at the highest of production capacities for pharmaceutical manufacturing campaigns and reported BX-LLE employed in experimental demonstrations did not describe the required processing time. Batch processes typically require significant manual intervention (Plumb, 2005) and thus labour costs are expected to be considerable. Optimisation of BX-LLE (with respect to batch volumes, number of LLE tanks and batch scheduling) is not considered here, but will help lower operating costs; however, it is

unlikely that BX-LLE will perform comparably with CPM-LLE designs regarding their operational asset efficiencies.

The total cost of the plant designs is calculated as the sum of *CapEx* and the sum of inflation-adjusted $OpEx_{annual}$ over the plant lifetime.

$$Total\ Cost = CapEx + \sum_{k=1}^{t=20} \frac{OpEx_{annual}}{(1+y)^k} \tag{31}$$

A plant-operating lifetime of t = 20 yr and an interest rate y = 5% are considered. All *CapEx* is assumed to occur in year 0 and operation is assumed to begin in year 1.

Table 6: Material prices for reagents and components used in API synthesis and batch (BX-) and continuous (CPM-) LLE.

Type	**Material**	**Price** (GBP kg^{-1})	**Type**	**Material**	**Price** (GBP kg^{-1})
Reagent	Tropine **2**	16.91	LLE Component	HCl (aq.)	0.08
	DMF	3.15		NH_4Cl (aq.)	0.60
	Phenylacetyl chloride **3**	5.49		Buffer (pH 10)	0.60
	NaOH (aq.)	0.25		DCM	0.12
	Formaldehyde	1.89		Et_2O	1.59
	H_2O	0.60		*n*-BuOAc	0.86
				Toluene	0.56

2.3.6 Nonlinear Optimisation Formulation

The aim of the optimisation problem is to minimise plantwide total costs for atropine CPM. The objective function (eq. 32) of the nonlinear optimisation problem is the total cost (eq. 31) with LLE solvent to feed ratio (r, mass basis) and LLE tank volume as decision variables, both of which affect LLE phase properties and efficiency (E_{LLE}).

$$\min\ Total\ Cost \tag{32}$$

s.t.

$$0.25 < r < 5 \tag{33}$$

$$0 < V_{LLE} \tag{34}$$

The optimisation problem is solved in MATLAB using the built-in solver fmincon, implementing the (default) interior-point algorithm with tolerances of 10^{-6}. The problem was solved for all individual combinations of LLE solvent = {Et_2O, *n*-BuOAc, toluene}, plant capacity, Q_{API} = {10^3, 10^4} kg API yr^{-1} and assumed solvent recovery, SR = {30%, 50%, 70%}, i.e. 18 problem instances, to avoid mixed integer problem formulations and reduce optimisation problem complexity.

Multiple initial values for decision variables are used to ensure a unique optimal solution for each problem instance. Initial values for LLE tank volume ($V_{LLE,0}$) and LLE solvent-to-feed ratio (r_0) are provided in Table 7. Initial tank volumes vary with selected plant capacity to account for varying material throughputs. A total of 12 initial points per problem instance is considered. Unique solutions were attained for all problem instances for different initial values of decision variables.

Table 7: Decision variable initial values for different plant capacities for atropine CPM optimisation.

Q_{API} (kg API yr^{-1})	$V_{LLE,0}$ (L)	r_0	# initial points per problem instance
10^3	{50, 100, 250, 500}	{1.0, 2.5, 4.0}	12
10^4	{500, 1,000, 2,500, 5,000}	{1.0, 2.5, 4.0}	12

3. Results and Discussion

3.1 Plug Flow Reactor (PFR) Design

Table 7 shows PFR design results corresponding to total cost minima under different assumptions of CPM-LLE solvent choice and plant capacity. Varying solvent recovery (*SR*) has little effect on resulting PFR volumes; *SR* varies only the solvent input and waste from the process, with internal material flows remaining roughly the same to meet a desired plant capacity for a particular LLE solvent choice. Therefore, average PFR volumes and lengths for all *SR* assumptions are shown. Computed PFR volumes are small for their respective capacities for all LLE solvent choices. For all cases, $V_{PFR1} < V_{PFR2}$ due to the higher conversion achieved within a shorter residence time as demonstrated in the experimental continuous flow synthesis (Bédard *et al.*, 2016). Reactor volumes are approximately an order of magnitude larger at $Q_{API} = 10^4$ kg API yr^{-1} compared to $Q_{API} = 10^3$ kg API yr^{-1}, reflecting the similar increase in product output. For both capacities, PFR volumes are smallest with toluene usage as the LLE solvent, followed by Et_2O and then *n*-BuOAc; this is due to the decreasing API retention in the product aqueous phase in the LLE process as characterised by the published values of API partition coefficient between organic and aqueous phases for the systems considered here (Bédard *et al.*, 2016).

Table 8: Plug flow reactor (PFR) design results for different CPM-LLE solvent implementations.

CPM-LLE Solvent = Et_2O								
Q_{API} (kg API yr^{-1})			**10^3**			**10^4**		
Reactor	**Temperature** (°C)	X_A (%)	V_{PFRi} (mL)	**Diameter** (mm)	**Length** (m)	V_{PFRi} (mL)	**Diameter** (mm)	**Length** (m)
PFR-1	100	99	159	5.0	8.08	1,511	5.0	76.94
				10.0	2.02		10.0	19.24
				20.0	0.50		20.0	4.81
				50.0	0.08		50.0	0.77
PFR-2	100	78	256	5.0	13.04	2,438	5.0	124.15
				10.0	3.26		10.0	31.04
				20.0	0.82		20.0	7.76
				50.0	0.13		50.0	1.24
CPM-LLE Solvent = *n*-BuOAc								
Q_{API} (kg API yr^{-1})			**10^3**			**10^4**		
Reactor	**Temperature** (°C)	X_A (%)	V_{PFRi} (mL)	**Diameter** (mm)	**Length** (m)	V_{PFRi} (mL)	**Diameter** (mm)	**Length** (m)
PFR-1	100	99	167	5.0	8.48	1,562	5.0	79.57
				10.0	2.12		10.0	19.89
				20.0	0.53		20.0	4.97
				50.0	0.08		50.0	0.80
PFR-2	100	78	269	5.0	13.69	2,521	5.0	128.39
				10.0	3.42		10.0	32.10
				20.0	0.86		20.0	8.02
				50.0	0.14		50.0	1.28
CPM-LLE Solvent = Toluene								
Q_{API} (kg API yr^{-1})			**10^3**			**10^4**		
Reactor	**Temperature** (°C)	X_A (%)	V_{PFRi} (mL)	**Diameter** (mm)	**Length** (m)	V_{PFRi} (mL)	**Diameter** (mm)	**Length** (m)
PFR-1	100	99	153	5.0	7.77	1,447	5.0	73.68
				10.0	1.94		10.0	18.42
				20.0	0.49		20.0	4.61
				50.0	0.08		50.0	0.74
PFR-2	100	78	246	5.0	12.53	2,335	5.0	118.89
				10.0	3.13		10.0	29.72
				20.0	0.78		20.0	7.43
				50.0	0.13		50.0	1.19

Table 8 also shows resulting PFR lengths for different assumptions of PFR inner diameter. Selection of appropriate reactor dimensions is essential to ensure adequate heat and mass transfer efficiencies are maintained (Zhang *et al.*, 2017); however, while smaller inner diameters are better for enhanced heat and mass transfer and mixing, resulting PFR lengths must also be feasible. Reactor diameter ranges (5-25 mm) consistent with our previous publications (Diab and Gerogiorgis, 2017, 2018a, Jolliffe and Gerogiorgis, 2017a, 2017b) have been selected for PFR design. At lower

capacities (Q_{API} = 10^3 kg API yr^{-1}), smaller diameters (5-10 mm) are feasible, whereas higher plant capacities (Q_{API} = 10^4 kg API yr^{-1}) require larger diameters to allow feasible reactor lengths. Minimisation of plant footprint is possible by coiling PFRs to allow more compact designs (Mascia *et al.*, 2013).

3.2 Continuous Liquid-Liquid Extraction (CPM-LLE) Design

Figure 9 shows CPM-LLE tank volumes and efficiencies corresponding to total cost minima under different design assumptions. For both plant capacity assumptions, CPM-LLE tank volumes are smallest when Et_2O is used as the LLE solvent, closely followed by toluene usage, with tank volumes for *n*-BuOAc usage being considerably larger. Smaller tank volumes are required for Et_2O and toluene due to their improved retention of API in the product aqueous phase as per the published values of API partition coefficient between organic and aqueous phases and stronger phase splitting observed in the ternary solvent systems for the solvent systems (Fig. 8) considered here (Bédard *et al.*, 2016); as API retention is better for these solvent systems, smaller LLE volumes are required to attain desired plant capacities, which is favourable for minimising total cost contributions as per the optimisation problem formulation. Tank volumes and LLE efficiencies decrease as the assumed solvent recovery increases; when more solvent is recovered, the process becomes both more materially- and economically-efficient (lower waste costs = lower *OpEx*) and thus the same plant capacity can be achieved by operating with smaller tanks and resulting lower LLE efficiencies.

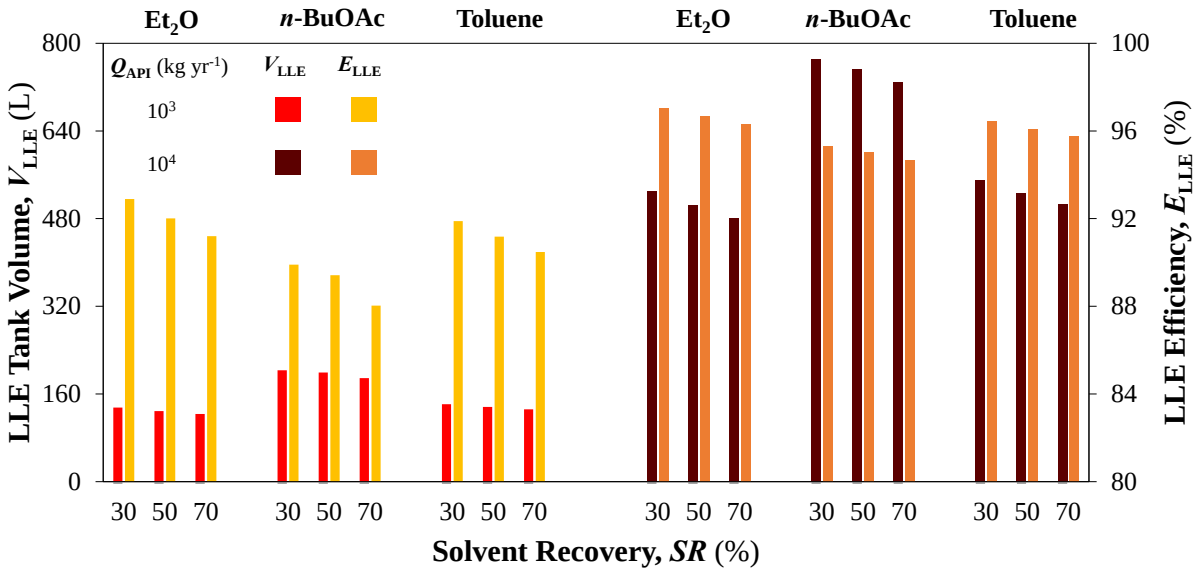

Figure 9: Cost optimal continuous liquid-liquid extraction (CPM-LLE) designs for different design assumptions.

The CPM-LLE solvent-to-feed ratio (*r*) is pushed to the lower bound of 0.25 in all design cases. Addition of LLE solvent is more influential on the properties of phases, tank residence time and LLE efficiency than it is on retention of API in the aqueous product phase, i.e., plantwide API recovery. Addition of LLE solvent also affects impurity removal into the organic phase. It is likely that there will be a maximum impurity content allowed in the aqueous mixture prior to subsequent API crystallisation; quantification of such limits could be incorporated as additional constraints and allow recasting of the problem for multiobjective optimisation. Further knowledge of purity and processing requirements prior to subsequent atropine crystallisation from this aqueous stream will inform further CPM development. Validity of the optimal design and operating parameters presented here are for the stated plant capacities, solvent recoveries and LLE solvent choices; implementation of process analytical technology (PAT) is essential to ensure optimal process design results presented here to realise their cost optimal benefits for successful CPM implementation (Eldin *et al.*, 2016; Yu and Kopcha, 2017).

Designs for CPM-LLE here assume a single tank implementing the desired purification. The consideration of multiple LLE tanks in series with comparative evaluation of crosscurrent (suitable for

small scale applications) and countercurrent (economical solvent usage) flow arrangements has not been considered here but can further elucidate CPM benefits for atropine production. Splitting the PFR-2 effluent into multiple feeds for separate LLE tanks is also a possibility that would provide additional operational flexibility; consideration of these design variations in future work will further clarify potential promising operating configurations for atropine CPM.

3.3 API Recoveries, *E*-Factors and Impurity Partitioning

Figure 10 shows attained API recoveries and *E*-factors corresponding to total cost minima under different design assumptions. The recovery attainable when implementing BX-LLE (assumed to be 99% for all as reported in the experimental demonstration (Bédard *et al.*, 2016) and for all considered capacities and solvent recoveries) is significantly higher than those attained via CPM-LLE design options; however, corresponding *E*-factors for BX-LLE is very high for all solvent recovery options.

For CPM-LLE designs, the highest recoveries, and correspondingly lowest *E*-factors, are attained when using Et_2O, followed by toluene, followed by *n*-BuOAc as LLE solvent. API recoveries decrease with increasing solvent recovery; this shows that API recoveries do not need to be as high to attain desired API capacities when higher solvent recovery is attainable, i.e., the cost benefits of recycling solvent allow for lower recoveries. Solvent constitutes a large portion of the material throughput of the process; thus, higher solvent recoveries lead to substantially lower *E*-factors. The *E*-factors for the CPM-LLE are high here due to the material intensity of the designed process, but they are still acceptable for pharmaceutical processes, which can have *E*-factors as high as 200 (Roschangar, Sheldon and Senanayake, 2015) and present significant reductions when compared to BX-LLE processes. Operating CPM-LLE at a higher pH would mean less water addition via neutralisation is required prior to LLE, which would consequently lower the *E*-factor; however, safety and operability considerations of operating under highly alkaline conditions on large production scales must also be considered.

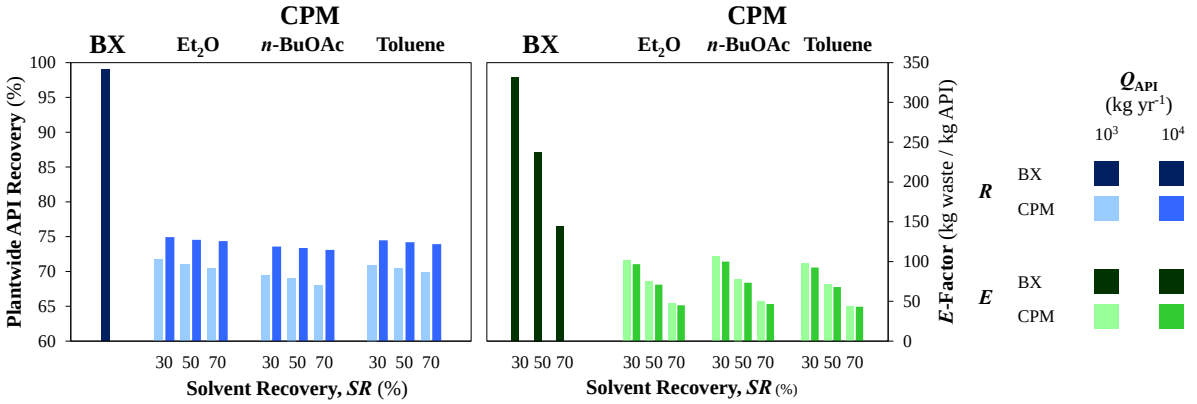

Figure 10: API recoveries and *E*-factors at cost optima of different design assumptions for plants with batch (BX)- and continuous (CPM)-LLE.

Figure 11 shows the ratio of API to impurity components (**2**, **5** and **6**) in CPM-LLE aqueous product streams at attained total cost minima under different design assumptions. API constitutes >60% of the solute content in the aqueous product stream (excluding NaCl, NaOH and H_2CO_3 present) in all cases; these are the most important solutes asides from the API, as selective crystallisation of API from the aqueous mixture over these impurities may be difficult in their presence due to their structural similarity to atropine. It is likely that there will be a maximum impurity content allowed in the aqueous mixture prior to subsequent API crystallisation; knowledge of such limits could be incorporated as additional constraints to the problem formulation. Further knowledge of such limits will elucidate additional cost contributions arising from further processing requirements, e.g., increased LLE equipment requirements and further LLE solvent addition, to clarify total cost components of different design configurations.

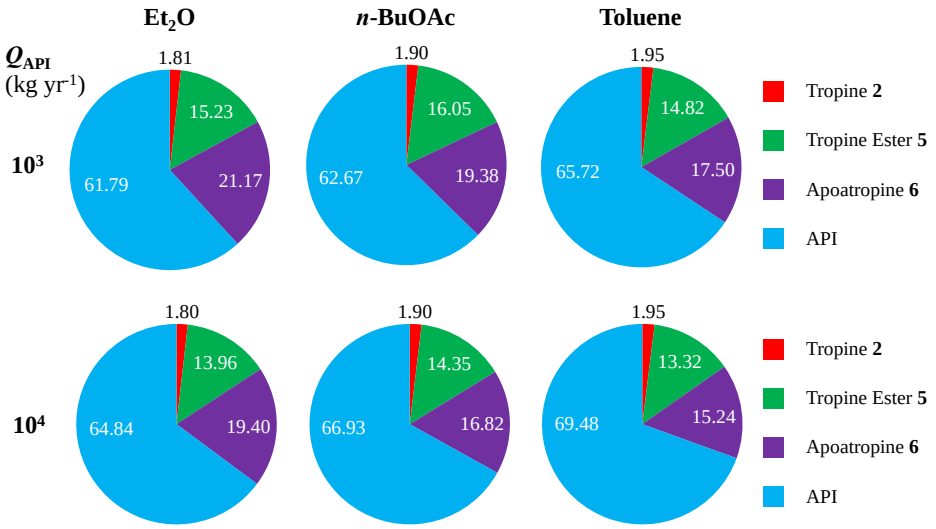

Figure 11: Molar ratios of API and impurities in product aqueous stream for different design assumptions.

It was previously mentioned that partition coefficient data used for calculation of API and impurity partitioning between phases assumes that organic phases are pure LLE solvent and aqueous phases are pure water. Real phases are multicomponent mixtures which affect the validity of this assumption. From the ternary phase diagrams for different solvent systems estimated from the UNIFAC model (Fig. 8), organic and aqueous product phases always contain <10 mol% DMF for all solvent systems considered here; however, neither phase is ever pure LLE solvent/water, and so the effect of the assumptions made when using published partition coefficient data in this work must be considered when interpreting the presented optimisation results.

3.4 Minimum Total Cost Components

Figure 12 shows minimum total cost components and contributions for different design assumptions. *OpEx* components decrease as solvent recovery increases due to reduced material requirement and waste costs; enhancing solvent recovery is shown to significantly lower total costs due to the large contribution solvent content makes towards total material throughput and the large contribution of *OpEx* towards total costs. Decreasing *OpEx* with increasing solvent recovery assumptions is also illustrated by correspondingly increasing *CapEx* contributions. Materials and waste costs remain fairly consistent with varying solvent recovery, whereas utilities costs remain fairly consistent as internal material flows remain roughly the same in order to meet desired plant capacities. Similarly, *CapEx* components remain fairly consistent with varying solvent recovery; internal flowrates remain the same despite different solvent recoveries, and thus unit sizes remain approximately constant. *BLIC* dominates *CapEx* in all cases due to expensive CPM equipment (Table 4) while material costs dominate *OpEx* due to expensive reagents (Table 6). Total costs are approximately an order of magnitude higher at Q_{API} = 10^4 kg API yr^{-1} than at the lower Q_{API} = 10^3 kg API yr^{-1}, reflecting the tenfold capacity increase.

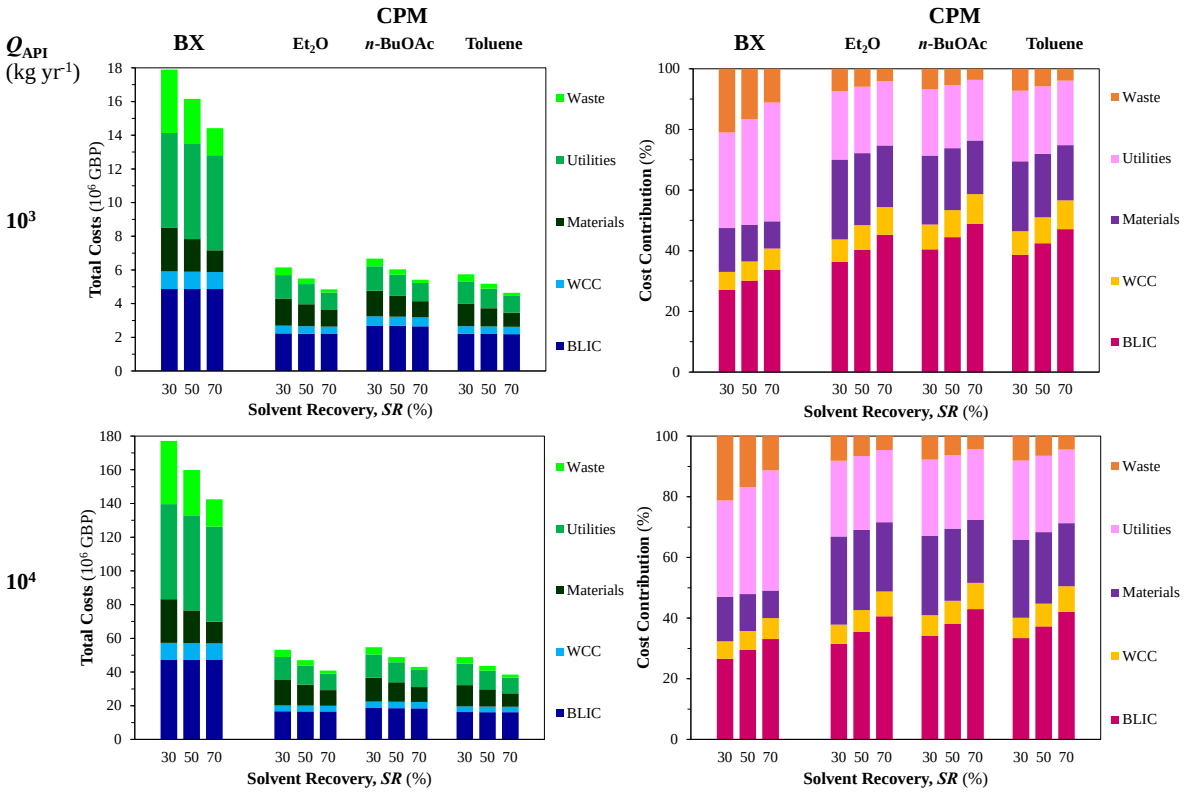

Figure 12: Minimum total cost components and contributions for different design assumptions.

Plant designs implementing BX-LLE are significantly higher than CPM-LLE for all design assumptions. *CapEx* components are higher due to the increase equipment requirements of BX-LLE compared to CPM-LLE processes (Figs. 6 and 7); *OpEx* components are higher due to the increased material requirements of BX-LLE compared to CPM-LLE. The increased material throughputs of BX-LLE are reflected in the high contribution of utilities to total BX-LLE costs. Table A1 (Appendix A) shows attained cost savings for different design assumptions (LLE solvent choice, plant capacity and solvent recovery) for CPM-LLE with respect to BX-LLE, which are significant for all cost components. The continuous LLE modelled in this work is a simplified version of the continuous separation implemented in the literature (Bédard *et al.*, 2016), which could not be modelled here due to the lack of explicit data on the performances of the implemented packed bed and membrane separator for reactor effluent purification (see section 2.3.3.1, Fig. 6). Our conceptual design has not been demonstrated in the literature and therefore optimisation results validation vs. experimental data is not possible. The presented results should be corroborated with experimenal investigation for validation and further elucidation of optimal design configurations for continuous atropine LLE.

Optimisation results show that toluene is the best LLE solvent choice, attaining the lowest total costs for all design cases presented. The next best LLE solvent is Et_2O, followed by *n*-BuOAc. Further corroboration of optimisation results with experimental validation as well as solvent harmonisation with crystallisation and other downstream processes is essential for atropine CPM development. Although toluene is more economically favourable, it has less favourable EHS criteria compared to *n*-BuOAc (Alder *et al.*, 2016). Explicit consideration of solvent selection heuristics based upon EHS criteria is not incorporated into the modelling and optimisation framework presented here; selection of LLE solvents in industrial practice will require consideration of EHS criteria as an integral part of the design process.

4. Conclusions

This work solves a novel nonlinear optimisation problem for the total cost minimisation of the continuous manufacturing of atropine, establishing promising plant designs with respect to LLE design and operating parameters. The implemented process model incorporates kinetic parameter estimation from experimental data for PFR design, UNIFAC modelling for ternary phase composition

and physical property estimation and published mass transfer correlations for LLE modelling and an established costing methodology for batch and continuous pharmaceutical processes. Optimisation of a conceptual continuous LLE for the purification of the API synthesis effluent following the continuous flow synthesis (Bédard *et al.*, 2016) for different LLE solvent choices and design assumptions (plant capacity and solvent recovery) are used to elucidate promising designs for atropine CPM. The LLE solvent-to-feed ratio (r) is driven to the lower bound in all design cases while LLE tank volumes vary between different design options due to its effect on LLE efficiency (affecting *OpEx* components) and *CapEx* contributions. Toluene emerges as the most economically favourable LLE solvent choice, offering significant total cost savings over batch LLE designs with acceptable material efficiencies for pharmaceutical manufacturing applications. Consideration of impurity limits in the LLE product aqueous stream and LLE solvent selection for harmonisation with subsequent crystallisation processes will provide further insight into optimal process configurations for atropine CPM. This work demonstrates the value of conducting technoeconomic optimisation studies towards the development of continuous processes in pursuit of economically viable end-to-end CPM plants. Industrial implementation and experimental validation of such efforts remain strategic R&D priorities: streamlining the use of lab- and/or pilot plant-scale reaction and separation experiments to guide the CPM process development effort is strongly recommended, especially via first-principles plantwide models which (in contrast to many data-driven ones) are applicable across all plant scales and sizes. Evaluating economic benefits systematically is of critical industrial importance, hence systematic modelling efforts can catalyse an accelerated and widespread adoption of continuous manufacturing.

Author Information

Corresponding Author
Email: D.Gerogiorgis@ed.ac.uk
Phone: + *44 131 6517072*
ORCID ID: Dimitrios I. Gerogiorgis: 0000-0002-2210-6784

Acknowledgements

Mr. Samir Diab gratefully acknowledges the financial support of the Engineering and Physical Sciences Research Council (EPSRC) via a Doctoral Training Partnership (DTP) PhD Fellowship (Grant # EP/N509644/1). Mr. Nikolaos Mytis and Prof. Andreas Boudouvis gratefully acknowledge financial support of Erasmus+ Student and Teaching Exchange Travel Scholarships from the National Technical University of Athens (NTUA) to the University of Edinburgh. Dr. Dimitrios I. Gerogiorgis gratefully acknowledges a Royal Academy of Engineering (RAEng) Industrial Fellowshp.

Appendix A: Continuous LLE Total Cost Component Savings

A cost savings comparison between CPM-LLE and BX-LLE plantwide designs is given in Table A1.

Table A1: Total cost components (10^6 GBP) with batch (BX) and continuous (CPM) LLE and CPM savings (%).

			Q_{API} = 10^3 kg yr^{-1}					
		BX	CPM					
			Et_2O		*n*-BuOAc		Toluene	
SR (%)	Component	**Cost**	**Cost**	**Savings**	**Cost**	**Savings**	**Cost**	**Savings**
30	*BLIC*	4.86	2.24	-53.97	2.70	-44.45	2.22	-54.35
	WCC	1.05	0.45	-56.90	0.54	-48.06	0.45	-57.30
	CapEx	5.91	2.69	-54.48	3.24	-45.09	2.67	-54.87
	Materials	2.59	1.62	-37.51	1.52	-41.38	1.32	-48.90
	Utilities	5.64	1.39	-75.38	1.46	-74.15	1.34	-76.30
	Waste	3.76	0.45	-87.98	0.45	-88.00	0.41	-88.95
	OpEx	11.98	3.46	-71.15	3.43	-71.41	3.07	-74.35
	Total Costs	17.89	6.15	-65.65	6.67	-62.72	5.74	-67.92
50	*BLIC*	4.86	2.21	-54.47	2.69	-44.77	2.20	-54.72
	WCC	1.05	0.45	-56.67	0.54	-47.49	0.44	-56.94
	CapEx	5.91	2.66	-54.85	3.23	-45.24	2.64	-55.11
	Materials	1.94	1.31	-32.83	1.24	-36.46	1.09	-44.15
	Utilities	5.64	1.20	-78.68	1.26	-77.71	1.16	-79.52
	Waste	2.68	0.33	-87.86	0.32	-87.93	0.30	-88.87
	OpEx	10.27	2.83	-72.40	2.82	-72.57	2.54	-75.27
	Total Costs	16.17	5.49	-66.00	6.04	-62.61	5.18	-67.92
70	*BLIC*	4.86	2.20	-54.82	2.65	-45.50	2.19	-55.02
	WCC	1.05	0.44	-56.29	0.53	-47.30	0.44	-56.50
	CapEx	5.91	2.64	-55.08	3.18	-45.81	2.63	-55.28
	Materials	1.30	0.99	-24.04	0.96	-26.14	0.84	-34.97
	Utilities	5.64	1.03	-81.75	1.08	-80.78	0.99	-82.48
	Waste	1.61	0.20	-87.75	0.20	-87.74	0.18	-88.78
	OpEx	8.55	2.21	-74.11	2.24	-73.79	2.01	-76.45
	Total Costs	14.42	4.85	-66.36	5.42	-62.40	4.64	-67.83
			Q_{API} = 10^4 kg yr^{-1}					
		BX	CPM					
			Et_2O		*n*-BuOAc		Toluene	
SR (%)	Component	**Cost**	**Cost**	**Savings**	**Cost**	**Savings**	**Cost**	**Savings**
30	*BLIC*	47.17	16.78	-64.42	18.65	-60.45	16.32	-65.40
	WCC	10.16	3.38	-66.70	3.76	-63.04	3.29	-67.66
	CapEx	57.33	20.17	-64.82	22.41	-60.91	19.60	-65.80
	Materials	25.88	15.49	-40.17	14.31	-44.70	12.60	-51.33
	Utilities	56.40	13.29	-76.43	13.75	-75.61	12.73	-77.43
	Waste	37.57	4.32	-88.49	4.25	-88.67	3.95	-89.48
	OpEx	119.85	33.10	-72.38	32.32	-73.03	29.28	-75.57
	Total Costs	177.18	53.27	-69.93	54.73	-69.11	48.88	-72.41
50	*BLIC*	47.17	16.68	-64.63	18.58	-60.60	16.23	-65.58
	WCC	9.98	3.36	-66.35	3.74	-62.55	3.26	-67.28
	CapEx	57.15	20.04	-64.93	22.32	-60.94	19.50	-65.88
	Materials	19.44	12.43	-36.07	11.62	-40.21	10.30	-47.01
	Utilities	56.40	11.44	-79.71	11.83	-79.02	10.96	-80.57
	Waste	26.83	3.10	-88.44	3.05	-88.64	2.83	-89.44
	OpEx	102.67	26.97	-73.73	26.50	-74.19	24.09	-76.53
	Total Costs	159.81	47.01	-70.58	48.82	-69.45	43.59	-72.72
70	*BLIC*	47.17	16.61	-64.79	18.50	-60.77	16.17	-65.72
	WCC	9.80	3.34	-65.93	3.72	-62.07	3.25	-66.85
	CapEx	56.97	19.95	-64.99	22.22	-60.99	19.42	-65.91
	Materials	12.99	9.35	-28.07	8.92	-31.31	7.98	-38.54
	Utilities	56.40	9.75	-82.71	10.08	-82.13	9.34	-83.45
	Waste	16.10	1.87	-88.40	1.84	-88.60	1.71	-89.40
	OpEx	85.49	20.96	-75.48	20.84	-75.62	19.03	-77.74
	Total Costs	142.45	40.91	-71.28	43.06	-69.77	38.44	-73.01

Nomenclature and Acronyms

Latin Letters and Acronyms

a	Interfacial area between LLE phases (m^2 m^{-3})
API	Active pharmaceutical ingredient
BLIC	Battery limits installed costs (GBP)
BX	Batch
C_i	Concentration of reagent *i* (M)
$C_{i,0}$	Initial concentration of reagent *i* (M)
CapEx	Capital expenditure (GBP)
CC	Contingency costs (GBP)
CEPCI	Chemical engineering plant cost index
CPM	Continuous pharmaceutical manufacturing
d_{32}	Sauter mean droplet diameter (m)
$D_{API,i}$	API diffusivity in phase *i* (m^2 s^{-1})
d_i	LLE tank impeller diameter (m)
d_t	LLE tank inner diameter (m)
DCM	Dichloromethane
DMF	Dimethylformamide
E	Environmental (*E*)-factor
E_{LLE}	LLE efficiency (%)
Eo	Eotvos number
Et_2O	Diethyl ether
f	Correction factor in eq. 20
Fr	Froude number
FOB	Free-on-Board Costs (GBP)
g	Acceleration due to gravity (= 9.81 m s^{-2})
IEC	Installed equipment costs (GBP)
K	Overall mass transfer coefficient (m s^{-1})
k_j	j^{th}-order reaction rate constant (varying units)
k_b	Boltzmann constant (=1.38064852 × 10^{-23} m^2 kg s^{-2} K^{-1})
k_i	Specific mass transfer coefficient of phase *i* (m s^{-1})
LLE	Liquid-liquid extraction
m_{API}	Mass of recovered API (kg yr^{-1})
$m_{process}$	Plant material throughput (kg yr^{-1})
m_{ur}	Mass of reagents remaining in waste streams (kg yr^{-1})
m_{uAPI}	Mass of unrecovered API (kg yr^{-1})
m_{uS}	Mass of unrecovered solvent (kg yr^{-1})
m_{waste}	Mass of waste (kg yr^{-1})
MAT_{annual}	Annual material costs (GBP yr^{-1})
n	Exponent in eq. 20
N_i	Impeller rotational speed (r.p.s.)
n-BuOAc	*n*-Butyl acetate
$OpEx_{annual}$	Annual operating expenditure (GBP yr^{-1})
P_j	Equipment purchase cost at capacity *j* (GBP)
Q_{API}	Plant API capacity (kg API yr^{-1})
Q_{LLE}	LLE volumetric throughput (m^3 s^{-1})
Q_{PFRi}	Volumetric flowrate through PFR *i* (m^3 s^{-1})
Q_{waste}	Volumetric flow of waste output (L yr^{-1})
PAT	Process analytical technology
PFR	Plug flow reactor
PPI	Process piping and instrumentation costs (GBP)
r	LLE solvent-to-feed ratio (mass basis)
r_0	Initial value for LLE solvent-to-feed ratio (mass basis)

R^2	Coefficient of determination
Re_i	LLE tank impeller Reynolds' number
S_j	Capacity of equipment *j* (varying units)
Sc_i	Phase *i* Schmidt number
Sh_i	Phase *i* Sherwood number
SR	Solvent recovery (%)
t	Plant operation lifetime (yr)
T_{LLE}	LLE operating temperature (25 °C)
$TPPC$	Total physical plant cost (GBP)
$UTIL_{annual}$	Annual utilities costs (GBP yr^{-1})
V_{LLE}	LLE tank volume (m^3)
$V_{LLE,0}$	Initial value for LLE tank volume (m^3)
V_{PFRi}	Volume of PFR *i* (m^3)
$Waste_{annual}$	Annual waste disposal cost (GBP yr^{-1})
WC	Working capital costs (GBP)
We	Weber number
WHO	World Health Organisation
x_{iS}^{j}	Component *i* mole fraction in phase *j* of solvent system *S*
X_A	Conversion of limiting reagent (%)
y	Interest rate (%)

Greek Letters

α	Coefficient in eq. 6
β	Coefficient in eq. 6
γ	Coefficient in eq. 6
Θ_i	Molar ratio of excess reagent *i* to limiting reagent
μ_i	Viscosity of phase *i* (kg m^{-1} s^{-1})
μ_m	LLE mixture viscosity (kg m^{-1} s^{-1})
ν_i	Stoichiometric coefficient of reagent *i*
ρ_i	Density of phase *i* (kg m^{-3})
ρ_m	LLE mixture density (kg m^{-3})
σ	Interphase surface tension (N m^{-1})
τ_{PFRi}	Residence time of PFR *i* (s)
ϕ	Dispersed phase volume fraction

References

Adamo, A., Beingessner, R.L., Behnam, M., Chen, J., Jamison, T.F., Jensen, K.F., Monbaliu, J.-C.M., Myerson, A.S., Revalor, E.M., Snead, D.R., Stelzer, T., Weeranoppanant, N., Wong, S.Y., Zhang, P., 2016, On-demand continuous-flow production of pharmaceuticals in a compact, reconfigurable system, *Science,* **352**(6281): 61–67.

Alder, C.M., Hayler, J.D., Henderson, R.K., Redman, A.M., Shukla, L., Shuster, L.E., Sneddon, H.F., 2016, Updating and further expanding GSK's solvent sustainability guide, *Green Chem.*, **18**(13): 3879–3890.

Anderson, N.G., 2012, Using continuous processes to increase production, *Org. Process Res. Dev.*, **16**(5): 852–869.

Angelopoulos, P.M., Gerogiorgis, D.I. and Paspaliaris, I., 2014, Mathematical modeling and process simulation of perlite grain expansion in a vertical electrical furnace, *App. Math. Model.* **38**(5-6): 1799–1822.

Bana, P., Örkényi, R., Lövei, K., Lakó, Á., Túrós, G.I., Éles, J., Faigl, F. and Greiner, I., 2017, The route from problem to solution in multistep continuous flow synthesis of pharmaceutical compounds, *Bioorg. Med. Chem*., **25**(23): 6180–6189.

Baumann, M. and Baxendale, I.R., 2015, The synthesis of active pharmaceutical ingredients (APIs)

using continuous flow chemistry, *Beilstein J. Org. Chem.*, **11**: 1194–1219.

Baxendale, I.R., Braatz, R.D., Hodnett, B.K., Jensen, K.F., Johnson, M.D., Sharratt, P., Sherlock, J.-P. and Florence, A.J., 2015, Achieving continuous manufacturing: technologies and approaches for synthesis, workup, and isolation of drug substance, *J. Pharm. Sci.*, **104**(3): 781–791.

Bédard, A.C., Longstreet, A.R., Britton, J., Wang, Y., Moriguchi, H., Hicklin, R.W., Green, W.H. and Jamison, T.F., 2016, Minimizing E-factor in the continuous-flow synthesis of diazepam and atropine, *Bioorg. Med. Chem.*, **25**(23):6233–6241.

Britton, J. and Raston, C.L., 2017, Multi-step continuous-flow synthesis, *Chem. Soc. Rev.*, **52**(5): 10159–10162.

Cole-Parmer, 2015, *Cole Parmer Polystat Advanced 15L Heat Cool Bath 35 to 200C 115VAC from Cole-Parmer United Kingdom*. Available at:

http://www.coleparmer.co.uk/Product/Cole_Parmer_Polystat_Advanced_15L_Heat_Cool_Bath_35_to_200C_115VAC/WZ-12122-56.

Cole, K.P., Groh, J.M.C., Johnson, M.D., Burcham, C.L., Campbell, B.M., Diseroad, W.D., Heller, M.R., Howell, J.R., Kallman, N.J., Koenig, T.M., May, S.A., Miller, R.D., Mitchell, D., Myers, D.P., Myers, S.S., Phillips, J.L., Polster, C.S., White, T.D., Cashman, J., Hurley, D., Moylan, R., Sheehan, P., Spencer, R.D., Desmond, K., Desmond, P. and Gowran, O., 2017, Kilogram-scale prexasertib monolactate monohydrate synthesis under continuous-flow CGMP conditions, *Science*, **356**(6343): 1144–1151.

Corning, 2015, *Corning Advanced-Flow G1 SiC Reactor*. Available at:

http://www.corning.com/media/worldwide/global/documents/G1_SiC_leaflet_FINAL_6.1.15.pdf.

Couper, J.R., 2003, *Process Engineering Economics*, CRC Press.

Dai, C., Snead, D.R., Zhang, P. and Jamison, T.F., 2015, Continuous-flow synthesis and purification of atropine with sequential in-line separations of structurally similar impurities, *J. Flow Chem.*, **5**(3): 133–138.

Dallinger, D. and Kappe, C.O., 2017, Why flow means green – Evaluating the merits of continuous processing in the context of sustainability, *Curr. Opin. Green Sust. Chem.*, **7**: 6–12.

Diab, S. and Gerogiorgis, D.I., 2017, Process modeling, simulation, and technoeconomic evaluation of separation solvents for the continuous pharmaceutical manufacturing (CPM) of diphenhydramine, *Org. Process Res. Dev.*, **21**(7): 924–946.

Diab, S. and Gerogiorgis, D.I., 2018a, Process modelling, simulation and technoeconomic evaluation of crystallisation antisolvents for the continuous pharmaceutical manufacturing of rufinamide, *Comput. Chem. Eng.*, **111**: 102–114.

Diab, S. and Gerogiorgis, D.I., 2018b, Process modelling, simulation and technoeconomic optimisation for continuous pharmaceutical manufacturing of (*S*)-warfarin, *Comput.-Aid. Chem. Eng.*, **43**: 1643–1648.

DiMasi, J.A., Grabowski, H.G. and Hansen, R.W., 2016, Innovation in the pharmaceutical industry: New estimates of R&D costs, *J. Health Econ.*, **47**: 20–33.

Drageset, A. and Bjørsvik, H.-R., 2016, Continuous flow synthesis concatenated with continuous flow liquid–liquid extraction for work-up and purification: selective mono- and di-iodination of the imidazole backbone, *React. Chem. Eng.*, **1**(4): 436–444.

EFPIA, 2018, The Pharmaceutical Industry in Figures, 28.

Eger, S. and Mahlich, J.C., 2014, Pharmaceutical regulation in Europe and its impact on corporate R&D, *Health Econ. Rev.*, **4**: 23.

Eldin, A.B., Ismaiel, O.A., Hassan, W.E. and Shalaby, A.A., 2016, Green analytical chemistry: Opportunities for pharmaceutical quality control, *J. Anal. Chem.*, **71**(9): 861–871.

Escotet-Espinoza, M.S., Rogers, A. and Ierapetritou, M.G., 2016, Optimization methodologies for the

production of pharmaceutical products, Humana Press, 281–309.

EvaluatePharma, 2018, *World Preview 2018*. Available at:

http://www.evaluategroup.com/public/Reports/EvaluatePharma-World-Preview-2018.aspx.

Federsel, H.-J., 2013, En route to full implementation: driving the green chemistry agenda in the pharmaceutical industry, *Green Chem*., **15**(11): 3105–3115.

Field, J.M., Hazinski, M.F., Sayre, M.R., Chameides, L., Schexnayder, S.M., Hemphill, R., Samson, R.A., Kattwinkel, J., Berg, R.A., Bhanji, F., Cave, D.M., Jauch, E.C., Kudenchuk, P.J., Neumar, R.W., Peberdy, M.A., Perlman, J.M., Sinz, E., Travers, A.H., Berg, M.D., Billi, J.E., Eigel, B., Hickey, R.W., Kleinman, M.E., Link, M.S., Morrison, L.J., O'Connor, R.E., Shuster, M., Callaway, C.W., Cucchiara, B., Ferguson, J.D., Rea, T.D. and Vanden Hoek, T.L., 2010, Part 1: Executive Summary: 2010 American heart association guidelines for cardiopulmonary resuscitation and emergency cardiovascular care, *Circulation*, **122**(18): S640–S656.

Fredenslund, A., Jones, R.L. and Prausnitz, J.M., 1975, Group-contribution estimation of activity-coefficients in nonideal liquid-mixtures, *AIChE J.*, **21**(6): 1086–1099.

Gérardy, R., Emmanuel, N., Toupy, T., Kassin, V.-E., Tshibalonza, N.N., Schmitz, M., Monbaliu, J.-C.M., 2018, Continuous flow organic chemistry: successes and pitfalls at the interface with current societal challenges, *Eur. J. Org. Chem.*, **2018**(2), 2301–2351.

Gerogiorgis, D.I. and Jolliffe, H.G., 2015, Continuous pharmaceutical process engineering and economics: Investigating technical efficiency, environmental impact and economic viability, *Chim. Oggi-Chem. Today*, **33**(6): 29–32.

Gillespie, D., 2007, Statistical simulation of chemical kinetics, *Ann. Rev. Phys. Chem.*, **58**: 35–55.

Goh, G.B., Hodas, N.O. and Vishnu, A., 2017, Deep learning for computational chemistry, *J. Comput. Chem.* **38**(16): 1291–1307.

Grom, M., Stavber, G., Drnovšek, P., Likozar, B., 2016, Modelling chemical kinetics of a complex reaction network of active pharmaceutical ingredient (API) synthesis with process optimization for benzazepine heterocyclic compound, *Chem. Eng. J.*, **283**: 703–716.

Gross, B. and Roosen, P., 1998, Total process optimization in chemical engineering with evolutionary algorithms, *Comput. Chem. Eng.* **22**: S229–S236.

Grujicic, M. and Chittajallu, K.M., 2004, Design and optimization of polymer electrolyte membrane (PEM) fuel cells, *Appl. Surf. Sci.* **227**(1-4): 56–72.

GSK, 2015, *GSK invests a further S$77mil to enhance antibiotic manufacturing facility in Singapore | GSK Singapore*. Available at: http://sg.gsk.com/en-sg/media/press-releases/2015/gsk-invests-a-further-s-77mil-to-enhance-antibiotic-manufacturing-facility-in-singapore/ (Accessed: 3 February 2016).

Henderson, R.K., Jiménez-González, C., Constable, D.J.C., Alston, S.R., Inglis, G.G.A., Fisher, G., Sherwood, J., Binks, S.P. and Curzons, A.D., 2011, Expanding GSK's solvent selection guide – Embedding sustainability into solvent selection starting at medicinal chemistry, *Green Chem*., **13**(4): 854–862.

Iervolino, A., 2016, *Pharmaceutical Innovation in Europe New pharmaceutical breakthroughs approaching-is the system set up to fund them all?* Available at: http://info.evaluategroup.com/rs/607-YGS-364/images/2016-EDF-Pharma-Innovation.pdf.

Jolliffe, H.G. and Gerogiorgis, D.I., 2016, Plantwide design and economic evaluation of two continuous pharmaceutical manufacturing (CPM) cases: ibuprofen and artemisinin, *Comput.-Aid. Chem. Eng*., **37**: 2213–2218.

Jolliffe, H.G. and Gerogiorgis, D.I., 2017a, Technoeconomic optimisation and comparative environmental impact evaluation of continuous crystallisation and antisolvent selection for artemisinin recovery, *Comput. Chem. Eng.*, **103**: 218–232.

Jolliffe, H.G. and Gerogiorgis, D.I., 2017b, Technoeconomic optimization of a conceptual flowsheet

for continuous separation of an analgaesic active pharmaceutical ingredient (API), *Ind. Eng. Chem. Res*., **56**(15): 4357–4376.

Kuehn, S.E., 2015, *Janssen Embraces Continuous Manufacturing for Prezista*, *Pharmaceutical Manufacturing*. Available at: http://www.pharmamanufacturing.com/articles/2015/janssen-embraces-continuous-manufacturing-for-prezista/.

Lee, S.L., O'Connor, T.F., Yang, X., Cruz, C.N., Chatterjee, S., Madurawe, R.D., Moore, C.M.V., Yu, L.X. and Woodcock, J., 2015, Modernizing pharmaceutical manufacturing: from batch to continuous production, *J. Pharm. Innov*., **10**: 191–199.

Ma, M., Lu, J., Tryggvason, G., 2015, Using statistical learning to close two-fluid multiphase flow equations for a simple bubbly system, *Phys. Fluids*, **27**:092101.

Marrs, T.C. and Rice, P., 2016, Chemical terrorism and nerve agents, *Medicine*, **44**(2): 106–108.

Mascia, S., Heider, P.L., Zhang, H., Lakerveld, R., Benyahia, B., Barton, P.I., Braatz, R.D., Cooney, C.L., Evans, J.M.B., Jamison, T.F., Jensen, K.F., Myerson, A.S. and Trout, B.L., 2013, End-to-end continuous manufacturing of pharmaceuticals: integrated synthesis, purification, and final dosage formation, *Angew. Chem.-Int. Ed.*, **52**(47): 12359–12363.

Monbaliu, J.C.M., Stelzer, T., Revalor, E., Weeranoppanant, N., Jensen, K.F. and Myerson, A.S., 2016, Compact and integrated approach for advanced end-to-end production, purification, and aqueous formulation of lidocaine hydrochloride, *Org. Process Res. Dev*., **20**(7): 1347–1353.

Patrascu, M. and Barton, P.I., 2018, Optimal campaigns in end-to-end continuous pharmaceuticals manufacturing. Part 2: Dynamic optimization, *Chem. Eng. Process*, **125**: 124–132.

Plenge, R.M., 2016, Disciplined approach to drug discovery and early development, *Sci. Transl. Med.*, **8**(349): 1–5.

Plumb, K., 2005, Continuous processing in the pharmaceutical industry - changing the mind set, *Chem. Eng. Res. Des.*, **83**(A6): 730–738.

Poechlauer, P., Colberg, J., Fisher, E., Jansen, M., Johnson, M.D., Koenig, S.G., Lawler, M., Laporte, T., Manley, J., Martin, B. and O'Kearney-McMullan, A., 2013, Pharmaceutical roundtable study demonstrates the value of continuous manufacturing in the design of greener processes, *Org. Process Res. Dev*., **17**(12): 1472–1478.

Poku, M.Y.B., Biegler, L.T., Kelly, J.D., 2004, Nonlinear optimization with many degrees of freedom in process engineering, *Ind. Eng. Chem. Res.* **43**(21): 6803–6812.

ProMinent, 2015, *Solenoid Driven Metering Pumps*. Available at: https://www.prominent.co.uk/en/Products/Products/Metering-Pumps/Solenoid-Driven-Metering-Pumps/pg-solenoid-driven-metering-pumps.html.

Rantanen, J. and Khinast, J., 2015, The Future of Pharmaceutical Manufacturing Sciences', *J. Pharm. Sci.*, **104**(11): 3612–3638.

Rogers, A. and Ierapetritou, M., 2014, Challenges and opportunities in pharmaceutical manufacturing modelling and optimization, *Comput.-Aid. Chem. Eng.*, **34**: 144–149.

Roschangar, F., Sheldon, R.A. and Senanayake, C.H., 2015, Overcoming barriers to green chemistry in the pharmaceutical industry – the Green Aspiration Level^{TM} concept, *Green Chem.*, **17**(2): 752–768.

Sheldon, R.A., 2012, Fundamentals of green chemistry: efficiency in reaction design, *Chem. Soc. Rev.*, **41**(4): 1437–1451.

Skelland, A.H.P. and Moeti, L.T., 1990, Mechanism of continuous-phase mass transfer in agitated liquid-liquid systems, *Ind. Eng. Chem. Res*., **29**(11): 2258–2267.

Teoh, S.K., Rathi, C. and Sharratt, P., 2015, Practical assessment methodology for converting fine chemicals processes from batch to continuous, *Org. Process Res. Dev*., **20**(2): 414–431.

Tryggvason, G., Ma, M., Lu, J., 2016, DNS-assisted modeling of bubbly flows in vertical channels,

Nucl. Sci. Eng., **184**: 312–320.

UK Office for National Statistics, 2016, *Business Enterprise Research and Development,* Available at:https://www.ons.gov.uk/economy/governmentpublicsectorandtaxes/researchanddevelopmentexpenditure/bulletins/businessenterpriseresearchanddevelopment/2016.

Weeranoppanant, N., Adamo, A., Saparbaiuly, G., Rose, E., Fleury, C., Schenkel, B. and Jensen, K.F., 2017, Design of multistage counter-current liquid–liquid extraction for small-scale applications, *Ind. Eng. Chem. Res*., **56**(14): 4095–4103.

Woods, D.R., 2007, *Rules of Thumb in Engineering Practice*, Wiley.

Yu, L.X. and Kopcha, M., 2017, The future of pharmaceutical quality and the path to get there, *Int. J. Pharmaceut*., **528**(1–2): 354–359.

Zhang, J., Wang, K., Teixeira, A.R., Jensen, K.F. and Luo, G., 2017, Design and scaling up of microchemical systems: a review, *Annu. Rev. Chem. Biomol.*, **8**: 285–305.